ORNL/TM-2022/2530

Development of A Microsampler for Aerial Collection of Aerosol Particles

Meng-Dawn Cheng
Chih-Hsiang Chien
David E. Graham
Andrew Harter

August 16, 2022

OAK RIDGE NATIONAL LABORATORY
MANAGED BY UT-BATTELLE FOR THE US DEPARTMENT OF ENERGY

ORNL/TM-2022/2530

Environmental Sciences Division

Development of A Microsampler for Aerial Collection of Aerosol Particles

Meng-Dawn Cheng[1]
Chih-Hsiang Chien[1]
David E. Graham[2]
Andrew Harter[3]

[1]Environmental Sciences Division,
[2]Biosciences Division,
[3] Geospatial Science and Human Security Division

Date Published: August 16, 2022

Prepared by
OAK RIDGE NATIONAL LABORATORY
Oak Ridge, TN 37831-6036
managed by
UT-BATTELLE, LLC
for the
US DEPARTMENT OF ENERGY
under contract DE-AC05-00OR22725

[THIS PAGE IS INTENTIONALLY LEFT BLANK.]

CONTENTS

ABSTRACT

A microsampler for aerosol particles was designed and evaluated in the laboratory for dry (no condensed water) and wet (foggy, misty, or rainy) air conditions. Computational Fluid Dynamics (CFD) results suggested a design that provided a higher sampling efficiency with minimal inlet loss. The microsampler was experimentally evaluated using fluorescent Polystyrene Latex (PSL) particles at four nominal sizes. The experimental results at the four PSL particle sizes agree reasonably well with the collection efficiencies predicted by CFD. We found no impacts on the collection efficiency of the microsampler at conditions under 80% Relative Humidity (RH). However, when condensed water exists, significant biases on the collection efficiencies were found suggesting this microsampler should not be used in the condition where there was condensed water in the atmosphere, e.g., foggy, misty, and rainy conditions.

1. INTRODUCTION

Sampling airborne particles, particulate matter (PM) or simply called "aerosol" from an unmanned aerial system (UAS), quadcopter, balloon, airship, drone, and dropsonde requires a very small sampler or collector. There are many commercial aerosol samplers in the market, but none that we know of meets the requirements for being an aerial aerosol sampler. Small footprint, lightweight, and low power consumption are three basic requirements, in addition, wireless communication may also be needed in some remote applications. This kind of aerosol sampling platforms have not been widespread and are mostly used in specialized applications.

Aerosol samplers designed for personal exposure studies are typically small. For example, the commercially available Sioutas five-stage cascade impactor (SKC, Inc.) was designed to collect respirable particles ranging from 0.25 to 10 μm at the flow rate of 9 liters per minute (LPM) [Misra et al. (2002)]. The impactor is reasonably small with an overall dimension of 8.6 cm x 5.5 cm and weights 159 g, (https://www.skcinc.com/products/sioutas-five-stage-cascade-impactor). The impactor (i.e., the main collector body itself) is small and lightweight, suitable for applications involving monitoring for human respiratory health. Such a collector would not be desirable for an aerial aerosol sampling application (e.g., Cheng, 2018) that requires a device with an overall volumetric dimension less than 8 cm^3 and weights less than 75 g, for example.

Furthermore, the Sioutas impactor, like all aerosol collectors, requires a vacuum pump which in turn requires a considerable amount of current through an alternating current (AC) or direct current (DC) power source (battery). The former of which is typically not an option for human health applications. A battery-powered pump, in general, would occupy a great portion of the overall system weight and size, because of the power requirement by the impactor operation. The power requirement is another important consideration in the design of an aerosol sampler for aerial UAS applications.

A few miniature aerosol sizers have been designed to meet the need of extremely small and light weight systems; thereby, these would be good candidates for aerial particle sampling. For example, a miniature virtual impactor designed to sample aerosol particles less than 2.5 μm was incorporated into an air-microfluidic sensor system (Paprotny et al., 2013). Several chip-based microfluidic sensors have been developed and tested for their toxicity measurements of aerosol particles, particularly when the toxic agents are causing oxidative stress. For example, Koehler et al. (2014) developed a microfluidic electrochemical sensor for measurement of the aerosol oxidative load, which could have the potential to be further developed into sensing other aerosol components. Brubaker et al. (2020) developed and applied a microfluidic device to investigate freezing properties of ice-nucleating particles. Liu et al. (2021) also explored the use of microfluidic online assay for aerosol oxidative potentials.

Microfluidic sensors require substantially smaller volumes of samples than traditional sensors for analysis and can provide near real-time results. Thus, they are ideal for airborne aerosol research applications. There has been limited development in micro aerosol samplers or collector. A quarter-sized miniature aerosol cyclone was designed to classify particles larger than 1 μm and 0.3 μm at 300 mL min^{-1} (Hsiao et al., 2009). Novosselov et al. (2014) developed a micro-channel collector and reported its performance at higher than 90% collection efficiency on particles greater than 1 μm by their single-loop micro-collector. Damit (2017) demonstrated a droplet-based microfluidic sensor for bioaerosol detection, with bioaerosol particles directly deposited into a droplet at the interface on a chip. With the advances in microfluidics detectors in the past couple of decades (Metcalf et al., 2018), the future development for microfluidics sensors that can be coupled to a microsampler is also expected to increase.

In this paper, we report a microsampler that was developed specifically for UAS applications. The size and weight are two main constraints of the collector, which is also required to collect aerosol particles of a size greater than 1 μm but less than 10 μm in aerodynamic diameter. The UAS is to be guided and directed into a target area of interest, remotely by wireless control. We shall discuss the design and experimental evaluation of the micro sampler in this paper, and leave out the application details, except to mention that the weight of the microsampler for our application is limited to no more than 50 g and overall dimension 2.5 cm x 2.5 cm x 1 cm. The sampling flow rate is restricted to 1 LPM. The sampling is to be accomplished with a DC-powered micropump.

2. METHODOLOGY

2.1 SAMPLER DESIGN CONCEPT

Figure 1a displays the schematic diagram of the microsampler. The concept of the design is adopted from the right-angle cascade impactors (Marple et al., 1995; Marple et al., 2003). Conventional impactor samplers such as the Micro-Orifice Uniform Deposition Impactor (MOUDI) has an inlet and outlet on opposite sides, and the aerosol is forced to make a 180-degree change in direction. However, the right-angle impactor has an unconventional flow pattern, and the flow must make two 90-degree turns to leave the system. For meeting the ultrasmall footprint and weight limitation, our microsampler described in this paper needs only a one-stage impaction as compared to the previous right-angle impactors that were slightly bulkier and heavier for our applications.

It is important for the design of a right-angle impactor that, after the flow leaves the impaction surface, the exit reduces the flow to achieve a lower velocity and prevent potential wall loss (Marple & Liu, 1974; Marple & Willeke, 1976; Marple et al., 1991; Marple et al., 1995; Marple et al., 2003). The following sections discuss the design of the impactor and the orifice.

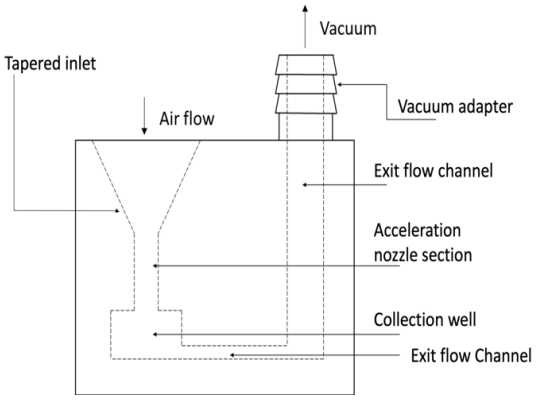

Figure 1a. Schematic diagram of a prototype micro aerosol sampler

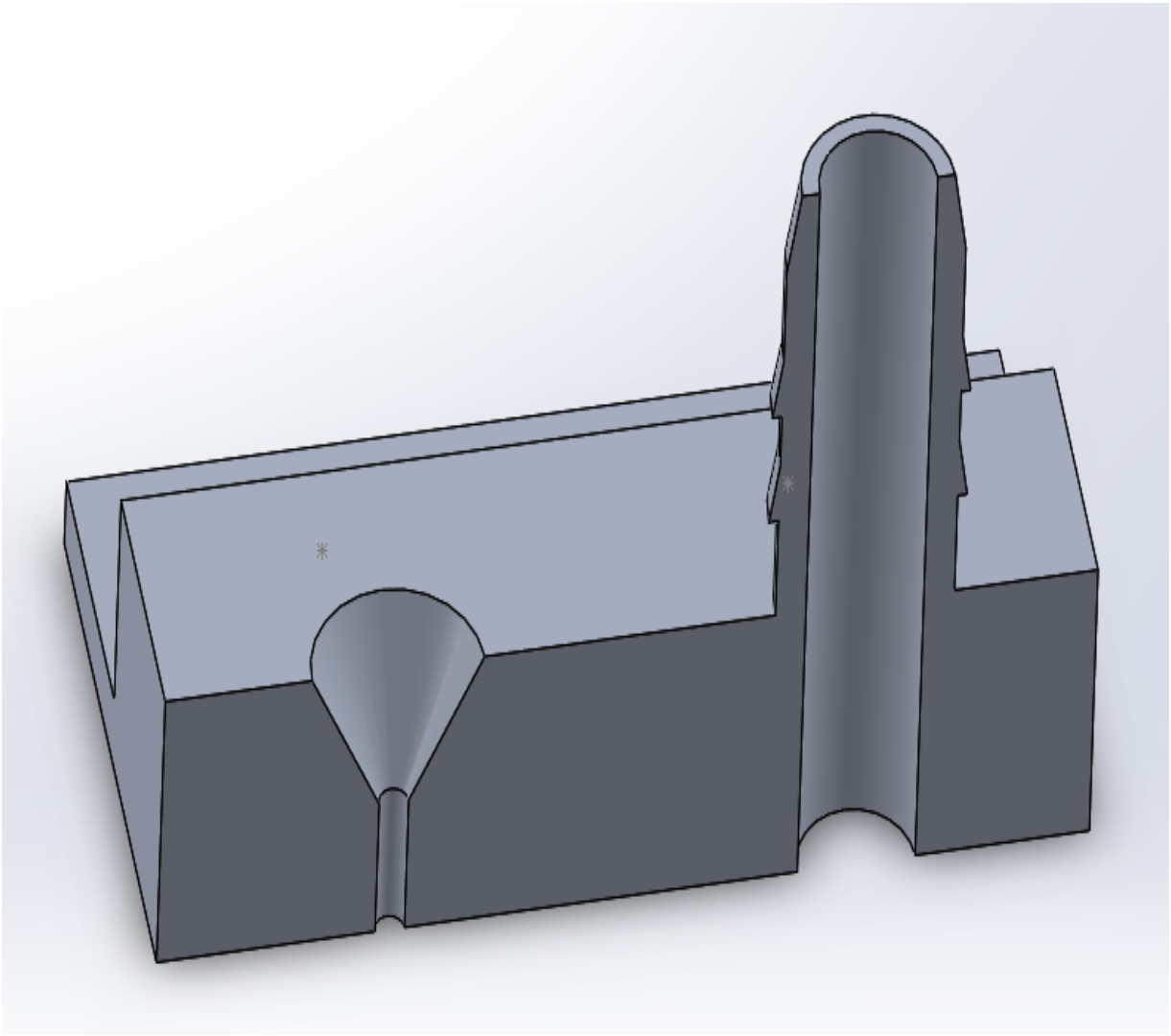

Figure 1b. 3D rendition of the tapered inlet

Figure 1c. Photo showing a 3D-printed Microsampler

2.1.1 General Consideration of the Impactor Design

Our sampler design follows the principle of virtual impaction in collection of aerosol particles. Impaction of particles on a collection substrate is determined by the Stokes' number of the particle. In other words, the particle transmission through an impactor is governed by the impactor theory derived previously by Marple & Liu (1974) and Marple & Willeke (1976) and formulated as follows:

$$St = \frac{\rho_p d_p^2 U C_c}{9\mu D_j}$$

where St is the Stokes number, ρ_p is particle density, d_p is the particle size, U is the free-stream jet velocity to the jet radius ($\frac{D_j}{2}$) of the impactor, and C_c is the Cunningham correction factor accounting for the particle slippage as their size becomes smaller than the mean free path of the air molecule, e.g., 0.6 μm at 20°C.

If the surface of the collection substrate is rigid, the Stokes number for 50% collection efficiency (St_{50}) is 0.24 for a circular jet. The cut size or cut diameter of the impactor for the particle having a 50% collection efficiency (d_{50}) can then be derived as:

$$d_{50}\sqrt{C_c} = \left[\frac{9\pi\mu D_j^3 (St_{50})}{4\rho_p Q}\right]^{0.5}$$

At the design flow rate (Q) of 1.0 liter per minute (LPM), the sampler with a circular jet diameter (D_j) of 0.8 mm will have a jet velocity of 3,316 cm/s, and the jet Reynolds number (Re) 1,759. At 20° C, the air viscosity is 1.81×10^{4} poise while the air density is 1.2×10^{-3} g/cm^3. Therefore, the designed cut size can be calculated as 0.97 μm, accordingly.

The impactor geometry, such as the dimension of jet-to-plate distance (S), can also influence the cut size and the collection efficiency curve (Marple & Liu, 1974). For example, Marple & Liu (1974) presented a detailed account of how an efficiency curve was affected by the particle size, jet Reynolds number, and or the ratio of the jet-to-plate distance to the nozzle dimeter (S/D_j). However, if the S/D_j was designed in the range from 1 to 10 and the Reynolds number in the 500 to 3,000 range, then the penetration curve is less sensitive to the S/D_j. Accordingly, our design value for the parameter S/D_j was chosen to be 1.875 to achieve the sharpest cut-off characteristics possible.

2.1.2 Effects of the Sampling Inlet

Like all aerosol samplers, the inlet geometry is important in the effective collection of aerosol particles. With the sampler requirement that it be airborne on an aerial moving platform like a quadcopter, it is also critical that our design minimizes the loss of particles during the collection. Two types of sampling inlets were constructed and numerically evaluated for sampling aerosol particles into the collector. The straight geometry in Figure 2a is convenient for machine fabrication, but such a design is more likely to focus particles closer to the centerline than an angled orifice, as shown in Figure 2b (Jurcik & Wang, 1995), and cause significant particle loss at the entrance of the inlet. We therefore

designed a tapered inlet with a 31-degree half angle (i.e., 3.25 mm at cone height and 4.7 mm at cone diameter).

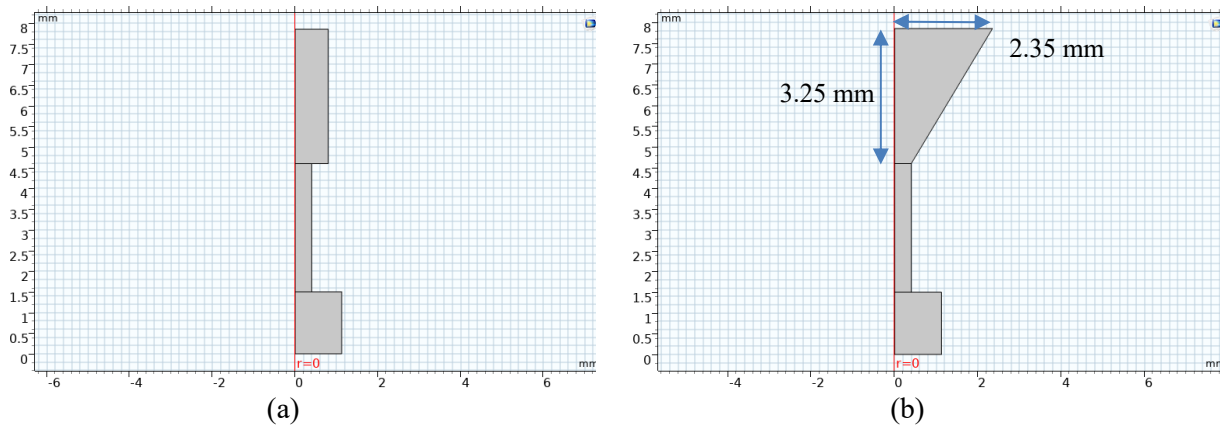

Figure 2. Impactor geometry with a) straight orifice and b) tapered orifice

The flow field and particle tracking analyses were conducted using the Computational Fluid Dynamics (CFD) module of the COMSOL Multiphysics V5.5 software. COMSOL solves the stationary general flow field by using a finite element method and fluid dynamics modules. The flow has a Reynolds number estimated to be 1,759. Particle tracking analysis was applied to produce the theoretical collection efficiency and visualize particle flow inside the collector. Using a symmetric, 2-D axisymmetric geometry as shown in Figure 2, the CFD modeling domain was discretized with a fine tetrahedral mesh.

An independence study using an extra fine-resolution mesh was conducted and the result are shown in Figure 3; the extra fine resolution composed of 20,064 tetrahedral node elements but did not yield significant differences in the estimated collection efficiency. Normal inflow velocity was applied on the inlet, and the design inlet flow rate was 1 LPM. Free boundary conditions were prescribed at the outlet (Hari et al., 2005). No-slip boundary condition was applied on the wall. The flow field was solved in a steady state. To capture the major and minor flow features, the quantitative convergence tolerance was achieved at 10^{-6} (Tu et al., 2018). The 50% collection efficiency cut-off was estimated at 0.97 µm as shown in Figure 3, consistent with the design value for the micro virtual impactor.

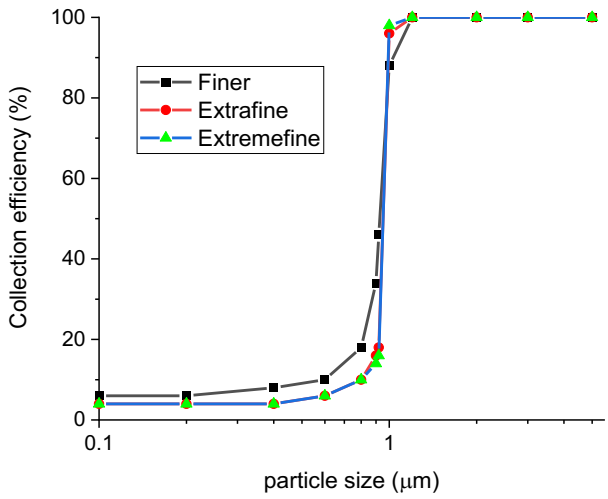

Figure 3. Collection efficiency curves for mesh independence study

Figure 4 shows the comparison between the velocity distributions of the two inlets. The flow fields of both inlets appear to be very similar, visually in Figure 4. However, a subtle difference exists and appears to be that a straight orifice led to a higher velocity (as shown in the darker red color) as the gas flow converged into the nozzle section. A higher flow velocity produces a larger inertia for larger particles, e.g., those larger than 50 μm, which could cause blockage to the micro inlet over a short time. Also, larger particle inertia could lead to particle bounce from the substrate as they impact onto during the collection. The higher converging velocity in the straight inlet could produce a higher loss of particles at the transition from the inlet section to the nozzle section, as we will be discussing in the subsequent sections during particle tracing analyses.

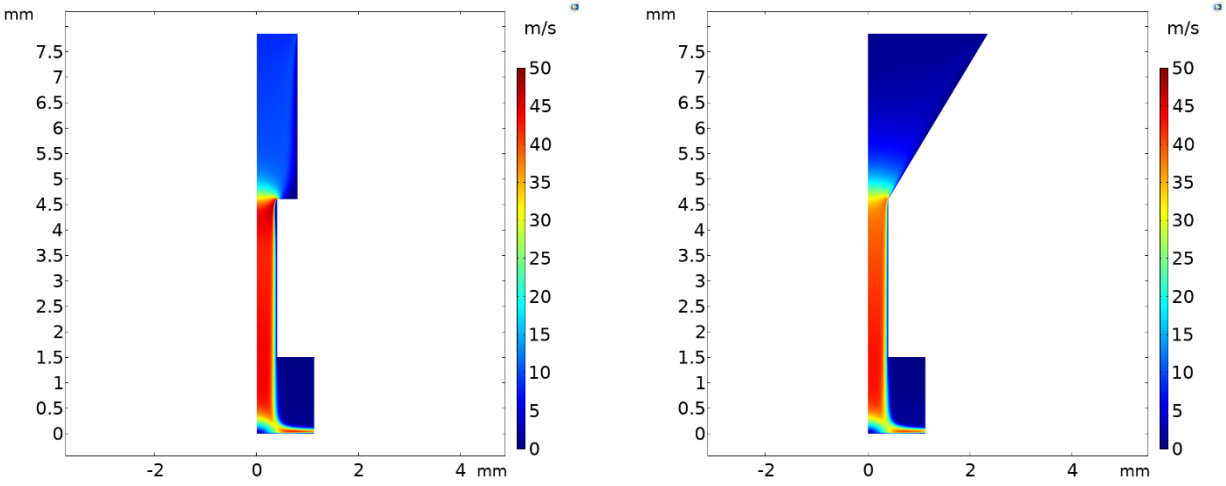

(a) (b)

Figure 4. Gas stream velocity profile for (a) straight orifice and (b) the tapered orifice

2.1.3 Evaluation of Collection Efficiency as a Function of Particle Size

To analyze the collection efficiency of the micro sampler, fifty (50) particles of the same size were used in the trajectory tracking. The size was varied in different simulations for the calculation of the collection efficiency for the selected size. These particles were injected uniformly from the top inlet boundary. Particles were then numerically sampled on the wall, substrate (i.e., particle impaction surface) at the bottom of the collection well, and outlet, they were counted as n_{wall}, $n_{substrate}$, and n_{oulet}, respectively. Note that particles were conserved to ensure all particle trajectories were tracked. The numerical collection efficiency ($\eta_{numerical}$) is defined in Eq. (1) as followings:

$$\eta_{numerical} = \frac{n_{substrate}}{n_{wall}+n_{substrate}+n_{outlet}} \quad \text{..... (1)}$$

Figure 5a shows the collection efficiency ($\eta_{numerical}$) curves numerically constructed for two inlet designs. For both straight and tapered inlets, the estimated 50% efficiency cut-off size was between 0.9 and 1 μm, within the tolerance of the designed value of 0.97 μm.

The difference in the geometry of the straight inlet causes insignificant impacts on the collection efficiency from that of the tapered inlet as shown in Figure 5a. Furthermore, the collection efficiency of the straight inlet decreases as the particle size (Dp) increases to be larger than the design cut size (Dpc) (see Figure 5a). The decrease in the collection efficiency for Dp > Dpc is dramatic. As shown in Figure 5a, it decreases from 100% for 1-µm particles to less than 70% for 5-µm ones, a 30% loss of collection efficiency. The loss of particles displayed in Figure 5b is another way to suggest the micro sampler should not be used for particles of size greater than the design cut off.

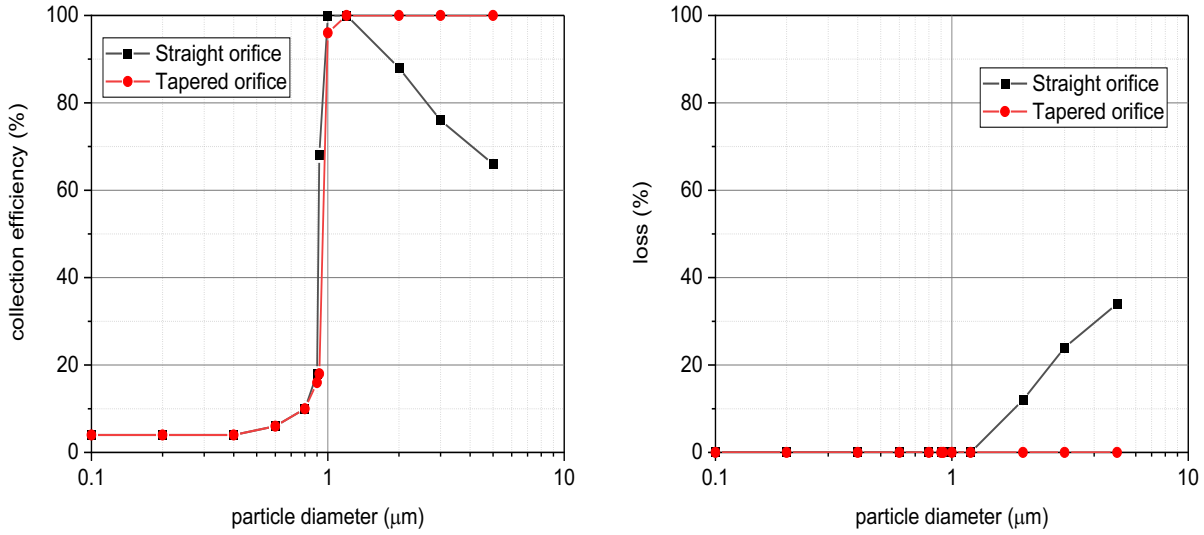

(a) (b)

Figure 5. (a) Collection efficiency curves and (b) particle loss for the two inlet designs

2.1.4 Particle Loss Analyses

Particle trajectory analysis was used for the analyses of particle loss and the results are shown in Figure 6. Two pairs of particle trajectory plots are presented in the figure for particles of two sizes, 1 and 3 µm. For 1- µm particles, the particle trajectories appear to be closer to the center axis as in the straight inlet (Figures 6a vs 6c). The particles sampled by the straight inlet thus were having higher momentum than those by the tapered inlet and would lead to uneven collection on the substrate as compared to the tapered inlet. This could contribute to an unwanted collection event (Jurcik & Wang, 1995). Additionally, it is important to note that the straight inlet can cause the loss of particles larger than 1 µm as discussed in the previous section. The loss increases as the particle size increases beyond the designed cut size of 1 µm (Figure 5b).

The particle trajectories in Figure 6b illustrate that 3-µm particles indeed deposited on the wall at the 90-degree angle turn during the transition from the inlet section to the acceleration nozzle section. This led to the particle loss we saw in the early section. The tapered inlet allows the particles to make a smooth transition into the acceleration nozzle section from the inlet section; therefore, all 3-µm particles were able to be collected on the center region of the substrate without random spreading on the substrate (see Figure 6d).

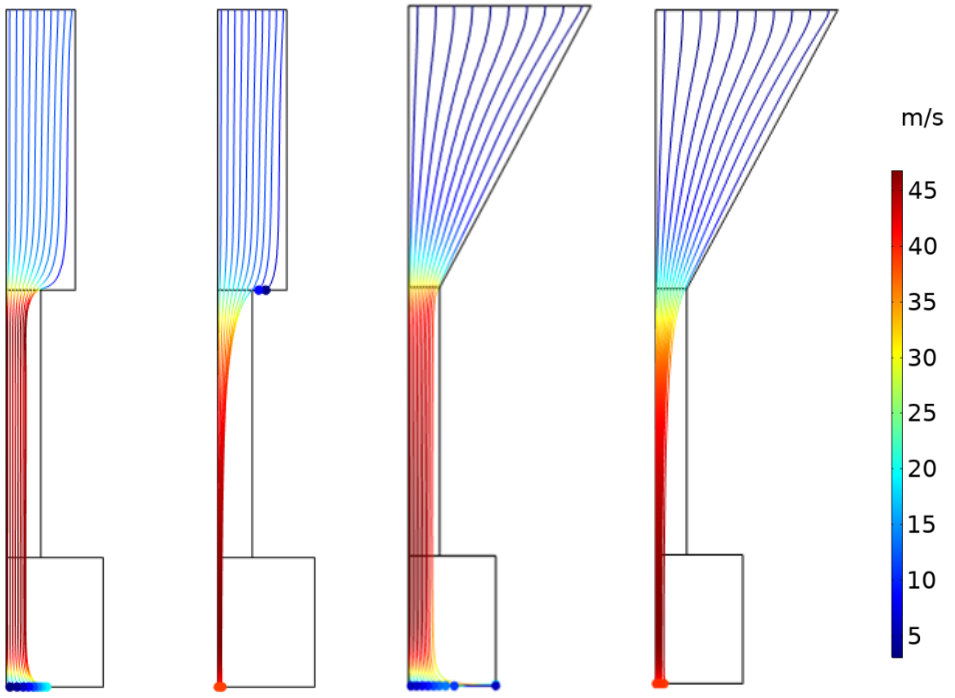

a) 1 µm b) 3 µm c) 1 µm d) 3 µm

Figure 6. 1-µm and 3-µm particle trajectories for straight and tapered inlets
(The color represents the velocity magnitude.)

2.2 PERFORMANCE EVALUATION – EXPERIMENTAL SETUP

The performance of the microsampler was evaluated, experimentally. We will describe the experimental setup in the following sections. Then, we will discuss the performance of the evaluation using latex spherical particles first and subsequently present the collection result of the micro sampler using bioaerosols in Chapter 3.

2.2.1 Aerosolization of PolyStyrene Latex (PSL) Particles

Commercially available fluorescent polystyrene latex (PSL) particles (Fluoresbrite®, YG Microspheres) from Polysciences, Inc. was used. The nominal diameters of the four monodisperse PSL particles were 0.5 µm, 0.75 µm, 1.0 µm, and 3.0 µm. These geometric sizes were taken as reported by the vendor and not verified further in our lab. The sizes were benchmarked, however, using a TSI Model 3021 Aerodynamic Particle Sizer (APS) in the aerosol state. Fluorescent particles were used in our study because the particle deposition pattern on the substrate in the sampler can be observed under a UV light.

Figure 7 shows the experimental setup for this study. The commercial fluorescent PSL suspension was diluted with Nanopure (18 Mω) to approximately 10^7 particles/mL and atomized in a 3-jet Collison nebulizer. HEPA-filtered building air was supplied to the Collison nebulizer to atomize the suspension to generate droplets. The relative humidity (RH) in the building air is generally 4%. The 26-psi HEPA-filtered air was supplied to the Collison nebulizer to generate droplets of the size with mass-median-diameter (MMD) approximately 2.5 µm (May, 1973) containing the PSL particles. Therefore, the supply

pressure was reduced to 20 psi to generate larger than 2.5- µm droplets that could effectively contain 3 µm solid PSL particles. Other than that, 26 psi supply pressure was used throughout for generating PSL particles of 0.5, 0.75, and 1 µm.

The nebulized aerosol flow was then directed to a diffusion dryer (TSI Model 3062) to remove water from the PSL particles in the process of forming dry solid PSL test particles. The 1st mixing jar was used to trap excess water before the diffusion dryer, also excess air was vented through a HEPA filter into a hood. A hygrometer (RH meter in Figure 7) was used to monitor the RH condition in the aerosol flow.

The aerosol particles after they pass the diffusion dryer were directed into the 2nd mixing jar that houses the micro sampler. The number concentration measured by the APS in the 2nd mixing jar (n_i) was used as the input concentration, while the number concentration measured at the outlet of the microsampler was used as n_o for the collection efficiency calculation [Eq. (2)]. Note that the APS pump was used to draw the aerosol particles into the 2nd mixing jar and through the microsampler if the 3-way valve was turned to permit flow through the micro sampler.

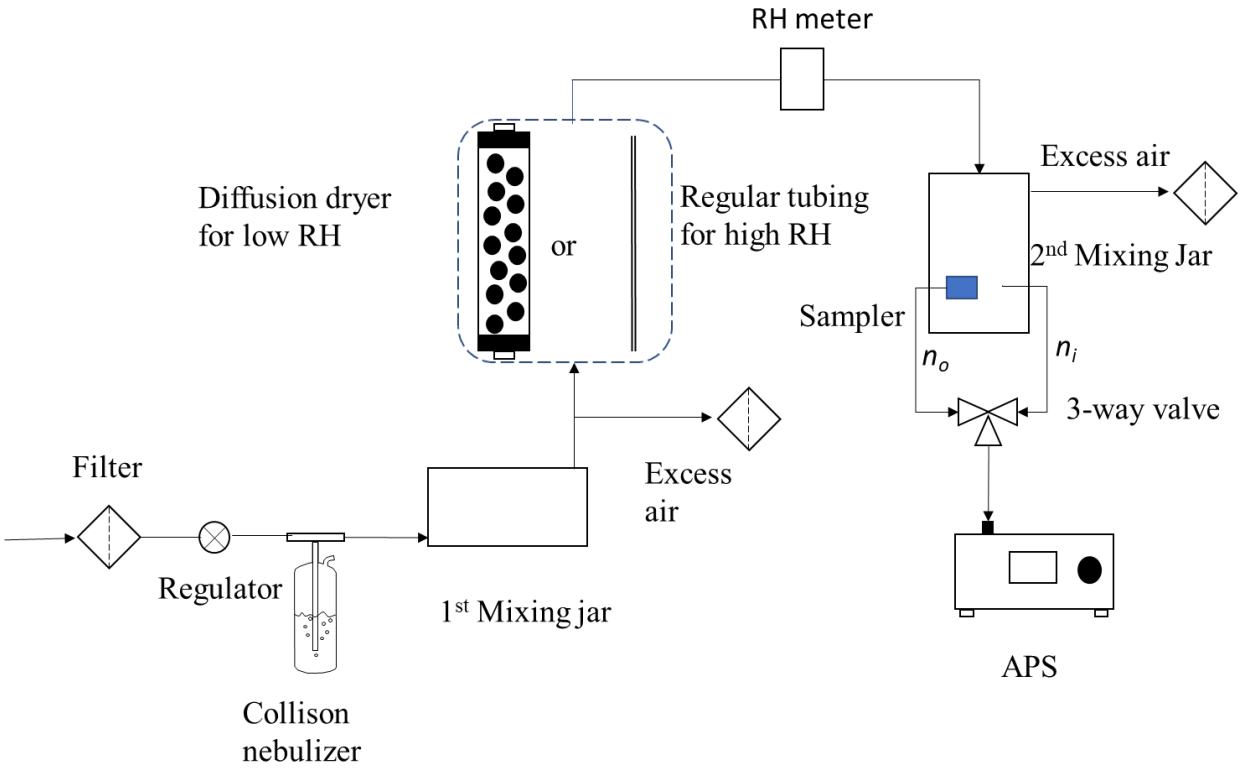

Figure 7. Experimental setup for collection efficiency evaluation

Again, the diffusion dried PSL particles were directed into a 2nd mixing jar for number concentration and size measurement by the APS (TSI model 3321). As an example, the 3-µm PSL particles population was showing an APS-measured size distribution in Figure 8 as the main peak. There was a smaller peak, with number concentration about ¼ size of the main peak, located at the proximity of 1 µm. We believe the small peaks could be attributed to the impurity of the prepared PSL suspension.

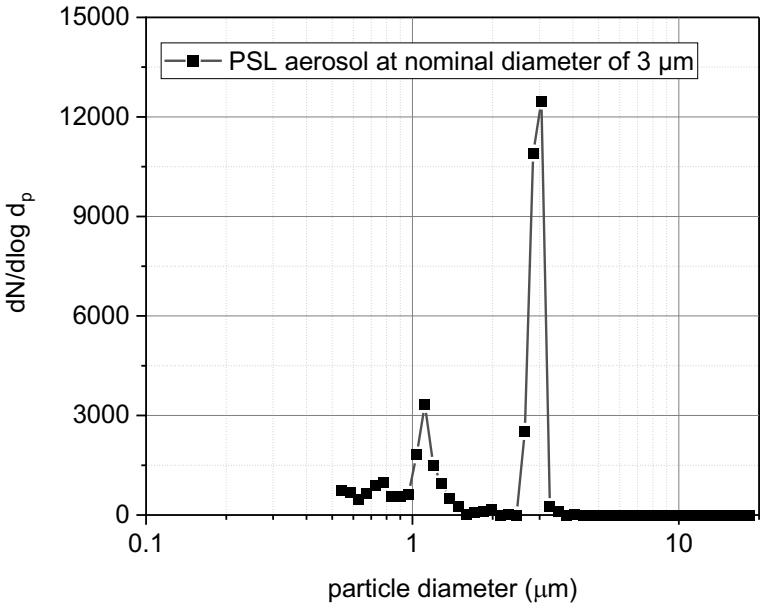

Figure 8. Size distribution of 3-µm PSL aerosol

The pressure drop through the sampler was measured with a differential pressure gauge (Dwyer Instruments, Inc.) as approximately 30.5 cm of water at 1 LPM. The flow rate Q_o of the microsampler was set at 1 LPM. The jar flow rate Q_i was slightly larger than Q_o, typically less than 1%. A correction factor (CF), Q_o / Q_i, was used to correct the calculated collection efficiency. However, the CF value is virtually identical to unity. Applying the correction factor CF, the experimental collection efficiency ($\eta_{experimental}$) was then computed as follows:

$$\eta_{experimental} = 1 - \frac{n_o}{n_i * CF} \quad \text{..... (2)}$$

2.2.2 Generation of Mists

To investigate the performance of the microsampler in a misty condition, a separate experimental setup was established. A misty condition is referring to atmospheric fog, drizzle, or rain drops. The Collison nebulizer used in the previous experiments generates liquid droplets with sizes much smaller than those found in the natural environment, ranging from 1 micron to a few millimeters (Seinfeld & Pandis, 2012), and at a number concentration, for example, 10^4 cm^{-3}.

We experimented with a different generation technique that allowed the production of larger liquid droplets in the size range that mimic those of natural liquid droplets in the atmosphere. Figure 10 shows the general setup for producing super-micrometer droplets for the experiments using an ultrasonic generator (Sono-Tek Corp.) with the same 0.5-µm fluorescent PSL particles.

The median droplet size (d_d) produced by the ultrasonic generator can be estimated from the following equation (Mahurin & Cheng, 2009):

$$d_d = 0.34\left(\frac{8\pi\sigma}{\rho f^2}\right)^{\frac{1}{3}}$$

where σ is the surface tension (N/m) of the liquid, ρ is the liquid density (Kg/m^3), and f is the operating frequency of the ultrasonic device in Hz. Assuming the generator was operated at 120 kHz, the median droplet size for water is estimated to be approximately 17 µm, which is in the right size range we were targeting.

Smaller droplets in the micron or submicron size range can rapidly evaporate, especially when mixing with dried purified air (water content at approximately 200 ppbv available from a ultradry air generator – Parker Balston Model UDA-300 Compressed Air Dryer) and disappear, while the sizes of large droplets were reduced somewhat as they travel down the chamber. Two positions (A and B in Figure 10) were used to test the effects of different droplet sizes on the collector performance. Position A is further down in the chamber than position B; thus, evaporation of water droplets will make the liquid droplets smaller at position A than that at position B, creating two size conditions for testing the interference of mists on the microsampler.

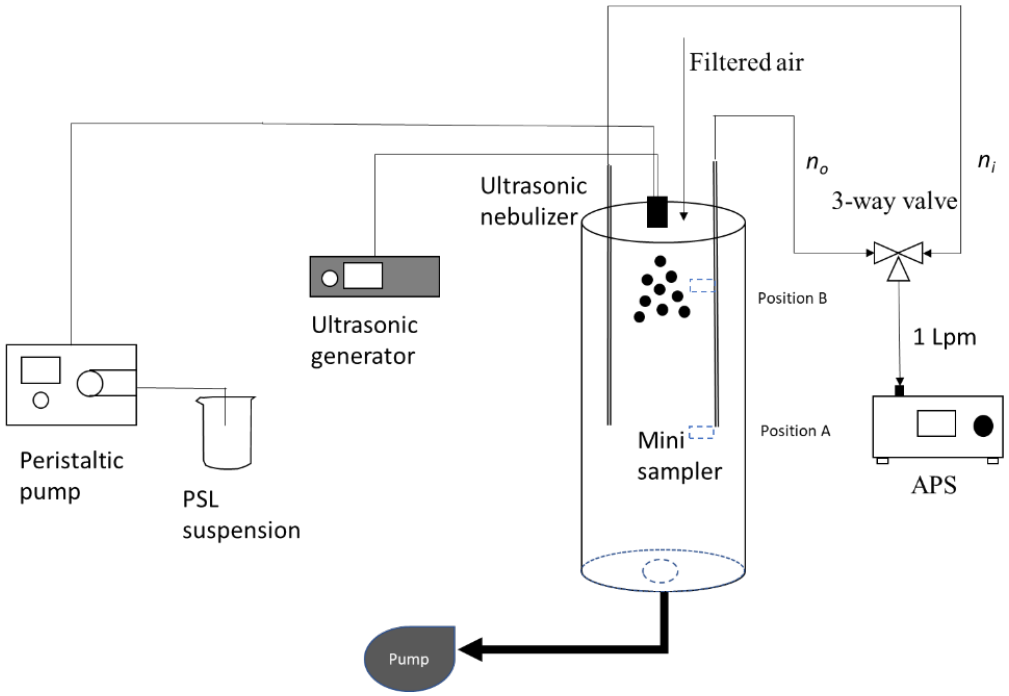

Figure 10. Experimental setup for the effects of mists on the collection efficiency

3. RESULTS AND DISCUSSION

3.1 Experimental Evaluation of Collection Efficiency Using Dried PSL Aerosol Particles

This section reports the experimental collection efficiency curve and compares it to the CFD results. The nominal PSL size reported by the vendor was slightly different from the aerodynamic diameter measured by the APS. Nominal diameters of 0.75 µm, 1.0 µm, and 3.0 µm were measured as 0.81 µm, 1.1 µm, and 2.9 µm in aerodynamic diameter, respectively. The APS does not measure the entire size distribution of the nominal 0.5 µm PSL, because the lower range of the measurement is approximately 0.5 µm. The APS 3321 was reported to have consistency issues between summing and correlated modes except for bin 1 (i.e., < 0.523 µm) (Peters & Leith, 2003). Therefore, the counts in bins 2 and 3 (i.e., 0.542 µm and 0.583) were selected and averaged to represent the particle counts at the size of 0.56 µm.

The experiments were conducted in the chamber at RH conditions of less than 30% under room temperature (ca. 20 °C). The predicted collection efficiency curve and collection efficiency calculated using experimental data for the microsampler is shown in Figure 11. The testing results for 1.1-µm particles showed the collection efficiency of 48±6% (n=18), which was close to the designed cut size at 0.96 µm. For particles of aerodynamic diameter of 2.9 µm, the collection efficiency was 97±0.3% (n=5). The collection efficiency for 0.56-µm particles was 9±9% (n=4) because of high penetration of particles smaller than the design cut size of 0.96 µm.

Although Figure 11 also shows that the experimental data generally agree with the predicted collection efficiency curve, the experimental collection efficiency for the 0.81-µm particles was 29±10% (n=22) while 10% collection efficiency was predicted. The efficiency for 1.1 um was predicted to be 99% while the experimental value was at 48±6%. In other words, 1.1 and 0.81-um diameters have uncertainty associated with the value. Thus, the characteristic curve of Figure 11 shows that the particle size at 50% removal efficiency to be 1 um within the tolerance of fabrication from the design cut size, although a better fabrication precision can be used in the future.

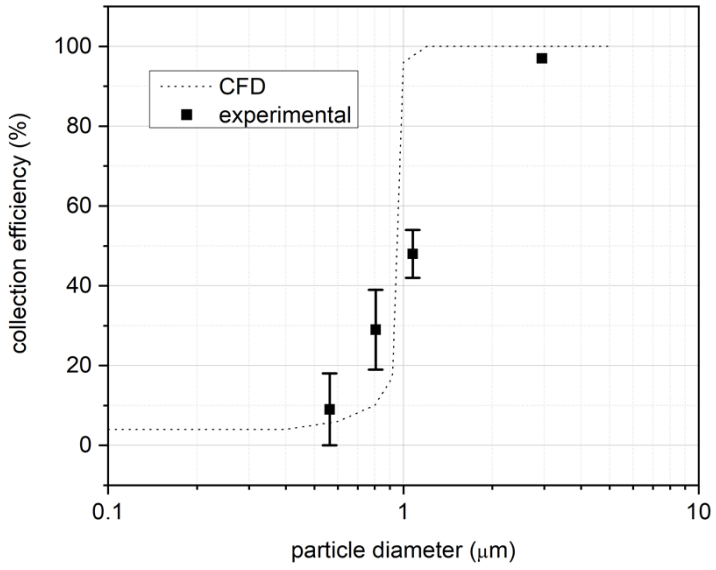

Figure 11. Particle collection efficiency curve from CFD and experimental data for the micro sampler at ≤ 30% RH

3.2 The Effect of High RH on the Collection Efficiency

Due to the small transport channel passage in this sampler, droplets in the misty, foggy, or cloudy air could pose detrimental effects on the sampler's performance. Furthermore, if a significant temperature gradient exists between the ambient air and the interior transport channel in the sampler, water vapor could condense on the channel wall and form droplets, potentially blocking the passageway, and thereby degrading the performance of the sampler. Thus, investigation of the humidity effect on the sampler performance is warranted.

The experimental setup for the investigation of humidity effects was like the experiment described in Section 2.2.1. A regular stainless-steel tube (see Figure 8) was used to replace the diffusion drier and maintain the RH in the aerosol stream at roughly 80%. Figure 12 shows an example of the particle size distribution for the low (≤ 30%) and high (80%) RH conditions. At lower humidity conditions (≤ 30% RH), only one peak was observed for the particle size distribution and all particles greater than the nominal size of around 0.5 µm were virtually unobservable. On the other hand, particles in the size range between 0.5 and 1.0 µm were observed by the APS at the conditions of 80% RH (see Figure 12) indicating the PSL particles were able to adsorb water vapor onto their surface thereby growing its size. Alternatively, the particles in the size range of 0.5 to 1.0 µm could simply be the water droplets that were unable to evaporate prior to sampling and measurement by the APS since the humidity condition in the aerosol stream was high (80% RH). These results demonstrate the aerosol population that exists under two different RH conditions given the same amount of PSL particles used in the suspension fed to the atomizer.

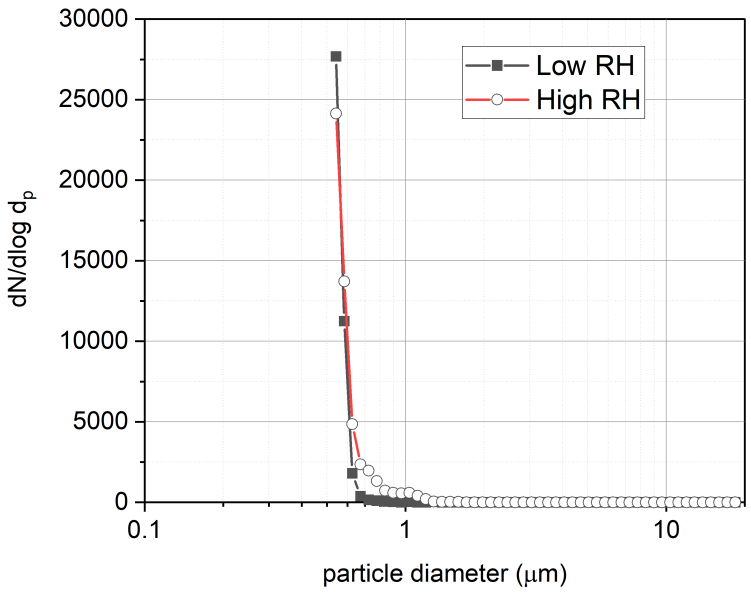

Figure 12. Size distribution of PSL aerosol at a nominal diameter of 0.5 µm for the low (≤ 30%) and high (80%) RH conditions

The collection efficiency of PSL aerosols which were 0.5 µm in size was compared at high RH conditions against the same system operated at low RH conditions. The collection efficiency was found to be 9±9% (n=4) for the low RH condition, while the collection efficiency was 9±10% (n=6) for the high RH condition. Therefore, the collection efficiency of this sampler for the 0.5-µm PSL particles appears to be statistically independent of atmospheric humidity up to 80% of our experimental boundary.

Furthermore, since the computational results, as displayed in Figure 5, show that the highest gas velocity inside the sampler was about 40 m/s, which is much slower than the speed of sound of 343 m/s at 20 °C, it is highly unlikely that the effect of aerodynamic cooling (Biswas et al., 1987) exists in this microsampler. We therefore do not expect water vapor to condense inside the micro sampler in a normal atmospheric environment. The sampler should maintain a collection performance close to that predicted for the environmental humidity condition of less than or equal to 80% RH.

3.3 The Effects of Mists on the Collection Efficiency

In the previous Sections, no condensed water exists in the aerosol stream in our experimental system. We now discuss the impacts of mists (condensed water) on the sampler performance in this section. APS counts for particles of 0.56-μm aerodynamic diameter were used to determine the collection efficiency. Recall that the collection efficiency of this microsampler for the particle size of 0.56 μm was 9±9% in the absence of mists as shown in Section 3.2. The collection efficiency for the particles increased to 38±3% (n=6) at the position B (farther away from the exit of the chamber), while the collection efficiency increased to 95% (n=2) at the position A (closer to the exit of the chamber). The presence of mists does not indicate the RH value in the chamber is 100%. The same 0.56-μm PSL aerosol population has another sub-population that is in the supermicron size range in a greater quantity at the position B than that at the position A as shown in Figure 13. Thus, the results appear to suggest that the sampler performance was impacted and biased by this subpopulation. In other words, the presence of condensed water in the air would significantly impact the sampling performance of this microsampler. Use of this microsampler should be restricted to the conditions where there is no condensed water existing in the atmosphere, simply no fog, no mist, and no rain in the air.

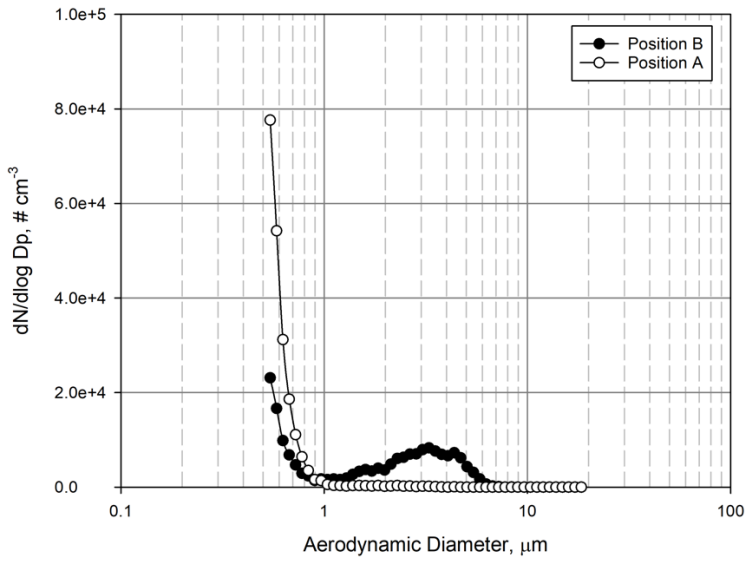

Figure 13. The size distribution of test aerosol populations in the test chamber at two sampling locations (A is the location closer to the chamber exit, while B is close to the inlet)

4. CONCLUSIONS

A microsampler for aerosol particles was designed and evaluated in laboratory for dry (no condensed water) and wet (foggy, misty, or rainy) air conditions. CFD results suggested a design that provided a higher sampling efficiency with minimal inlet loss. The microsampler was experimentally evaluated using fluorescent PSL particles at four nominal sizes. The experimental results at the four PSL particle sizes agree reasonably well with the collection efficiencies predicted by CFD. We found no impacts on the collection efficiency of the microsampler at conditions under 80% RH. However, when condensed water exists, significant biases on the collection efficiencies were found suggesting this microsampler should not be used in the condition where there was condensed water in the atmosphere, e.g., foggy, misty, and rainy conditions.

5. ACKNOWLEDGEMENTS

This research was supported by the Department of Defense/Defense Threat Reduction Agency. Chris Boring was acknowledged for assistance in the construction of the experimental chamber and Bart Murry was acknowledged for translating the CFD configuration into the CAD drawing and 3D-printing fabrication of the prototype sampler. Oak Ridge National Laboratory is managed by UT-Battelle, LLC for the U.S. Department of Energy under contract DE-AC05-00OR22725.

6. REFERENCES

Biswas, P., Jones, C. L., & Flagan, R. C. (1987) Distortion of size distributions by condensation and evaporation in aerosol instruments. *Aerosol Science and Technology*, *7*(2), 231-246.

Brubaker, T., Polen, M., Cheng, P., Ekambaram, V., Somers, J., Anna, S.L. & Sullivan, R.C. (2020) Development and characterization of a "store and create" microfluidic device to determine the heterogeneous freezing properties of ice nucleating particles, Aerosol Science and Technology, 54(1), 79-93.

Cheng, M.-D. (2018). Selective collection of airborne particulate matter. *Aerosol and Air Quality Research*, *18*(6), 1,361-1,365.

Damit, B. (2017) Droplet-based microfluidics detector for bioaerosol detection, Aerosol Science *and Technology*, 51:4, 488-500.

Hari, S., Hassan, Y. A., & McFarland, A. R. (2005). Computational fluid dynamics simulation of a rectangular slit real impactor's performance. *Nuclear Engineering and Design*, *235*(9), 1015-1028.

Hsiao, T.-C., Chen, D.-R., & Son, S. Y. (2009). Development of mini-cyclones as the size-selective inlet of miniature particle detectors. *Journal of Aerosol Science*, *40*(6), 481-491.

Jurcik, B., & Wang, H.-C. (1995). On the shape of impactor efficiency curves. *Journal of Aerosol Science*, *26*(7), 1139-1147.

Koehler, K. A., Shapiro, J., Sameenoi, Y., Henry, C., and Volckens, J. (2014) Laboratory evaluation of a microfluidic electrochemical sensor for aerosol oxidative load, *Aerosol Science and Technology*, 48(5), 489-497.

Liu, F., Ng, N.L. & Lu, H. (2021) Emerging applications of microfluidic techniques for in vitro toxicity studies of atmospheric particulate matter, *Aerosol Science and Technology*, 55(6), 623-639.

Mahurin, S. M., & Cheng, M.-D. (2009). Generating nanoscale aggregates from colloidal nanoparticles by various aerosol spray techniques. *Nanotoxicology*, *1*(2), 130-138.

Marple, V. A., & Liu, B. Y. H. (1974). Characteristics of laminar jet impactors. *Environmental Science & Technology*, *8*(7), 648-654.

Marple, V. A., Olson, B. A., & Miller, N. C. (1995). A low-loss cascade impactor with stage collection cups: calibration and pharmaceutical inhaler applications. *Aerosol Science and Technology*, *22*(1), 124-134.

Marple, V. A., Roberts, D. L., Romay, F. J., Miller, N. C., Truman, K. G., Van Oort, M., . . . Hochrainer, D. (2003). Next generation pharmaceutical impactor (a new impactor for pharmaceutical inhaler testing). Part I: Design. *Journal of aerosol medicine*, *16*(3), 283-299.

Marple, V. A., Rubow, K. L., & Behm, S. M. (1991). A microorifice uniform deposit impactor (moudi): description, calibration, and use. *Aerosol Science and Technology*, *14*(4), 434-446.

Marple, V. A., & Willeke, K. (1976). Impactor design. *Atmospheric Environment*, *10*(10), 891-896.

May, K. R. (1973). The collison nebulizer: Description, performance and application. *Journal of Aerosol Science*, *4*(3), 235-243.

Metcalf, A. R., Narayan, S., & Dutcher, C. S. (2018) A review of microfludic concept and applications for atmospheric aerosol science. *Atmospheric Science and Technology*, 52(3), 310-329.

Misra, C., Singh, M., Shen, S., Sioutas, C., & Hall, P. M. (2002). Development and evaluation of a personal cascade impactor sampler (PCIS). *Journal of Aerosol Science*, *33*(7), 1027-1047.

Novosselov, I.V., Gorder, R.A., Van Amberg, J.A. & Ariessohn, P.C. (2014) Design and Performance of a Low-Cost Micro-Channel Aerosol Collector, Aerosol Science and Technology, 48:8, 822-830

Paprotny, I., Doering, F., Solomon, P. A., White, R. M., & Gundel, L. A. (2013). Microfabricated air-microfluidic sensor for personal monitoring of airborne particulate matter: Design, fabrication, and experimental results. *Sensors and Actuators A: Physical*, *201*, 506-516.

Peters, T. M., & Leith, D. (2003). Concentration measurement and counting efficiency of the aerodynamic particle sizer 3321. *Journal of Aerosol Science*, *34*(5), 627-634.

Seinfeld, J. H., & Pandis, S. N. (2012). *Atmospheric chemistry and physics: from air pollution to climate change*. John Wiley & Sons.

Tu, J., Yeoh, G. H., & Liu, C. (2018). *Computational fluid dynamics: a practical approach*. Butterworth-Heinemann.